

# Semi-Rigid Floor-to-Wall Connections Using Side-Framed Lightweight Steel Structures: Concept Development

Alireza Bagheri Sabbagh<sup>a</sup>, Shahabeddin Torabian<sup>b</sup>

<sup>a</sup>School of Engineering, University of Aberdeen, Scotland, UK, alireza.bsabbagh@abdn.ac.uk

<sup>b</sup>Senior Project Consultant, Simpson Gumpertz & Heger, Inc. Washington DC, storabian@sgh.com

Adjunct Associate Research Scientist, Department of Civil and Systems Engineering, Johns Hopkins University, Maryland, Baltimore, USA

## Abstract

This paper presents the development of side-framed lightweight steel (SFLS) structures featuring semi-rigid floor-to-wall connections. Initially, the effect of variation of connection rotational stiffness on the design of a two-storey frame is investigated considering different construction methods. The results revealed a considerable effect of the connection rotational stiffness on the design of the joists and studs. A semi-rigid connection is then developed using validated finite element analyses. The developed SFLS system enables more efficient designs addressing the predominant limit states of the conventional designs with fewer and lighter flooring members and connections.

Keywords: Lightweight steel framing; Semi-rigid connections; Connection rotational stiffness.

## 1. Introduction

Typical best-practice lightweight steel framing (LSF) systems comprising cold-formed steel (CFS) stud walls and joisted floors include platform framing, ledger framing, and balloon framing [1]. These systems are being constructed using two different methods: (i) a sequential construction method (SCM) for platform and ledger framing, with floors and walls of one storey level built at a time with no stud continuity between the upper and lower storey walls, and (ii) a continuous construction method (CCM) for balloon framing, with the wall studs being spliced above the floor levels providing continuity between the adjacent storeys [1]. The flooring joists are either supported on top of the wall studs capped with a top track (in platform framing) or attached to the face of the walls (in both ledger and balloon framing). The floor-to-wall connections are generally categorised as simply supported designed to transfer shear or bearing forces to the wall frame [1-2]. The design of the joisted floors is generally dominated by the mid-span deflection serviceability limit state leading to relatively heavy flooring joists [1-3].

In recently completed experiments on ledger-framed LSF floor-to-wall connections [3] comprising floor joists connected to the face of the wall studs, various types of premature local failure limit states have been identified in the components of the floor-to-wall connections. These include ledger

34 flange buckling, stud web crippling, and fastener pull-out, which were identified as the dominant  
35 ultimate limit states [2]. These occur primarily due to the imposed eccentricity and the  
36 consequential out-of-plane actions within the floor-to-wall connection associated with the  
37 positioning of a single flooring joist relative to the location of adjacent wall studs. The identified limit  
38 states, which are not included in the current design practice, can compromise the gravity load-  
39 bearing system under extreme loading conditions [3]. To mitigate these failure limit states, a  
40 recommendation is to increase the stud thickness matching or greater than the joist thickness [3].  
41 This approach, however, can lead to an overly conservative design with a significant portion of  
42 underutilised strength of the stud sections.

43

44 A side-framed lightweight steel (SFLS) system comprising semi-rigid floor-to-wall connections is  
45 developed herein for a more efficient joist-stud framed design. The proposed system postpones or  
46 even eliminates local failure limit states within the connection components due to the zero  
47 eccentricity in the connection which has been identified as the primary source of the local failures in  
48 the ledger-framed connections. These local failures, as discussed above, could affect the design of  
49 the wall studs towards higher thickness sections [2]. The semi-rigid connections reduce the mid-span  
50 deflection of the joisted floors which has been recognised [3] as the governing limit state for the  
51 typical CFS floor systems. Furthermore, the SFLS system requires fewer number of members and  
52 connections, compared with the ledger-framed systems, eliminating a ledger beam per side of a wall  
53 and a clip angle connection per joist.

54

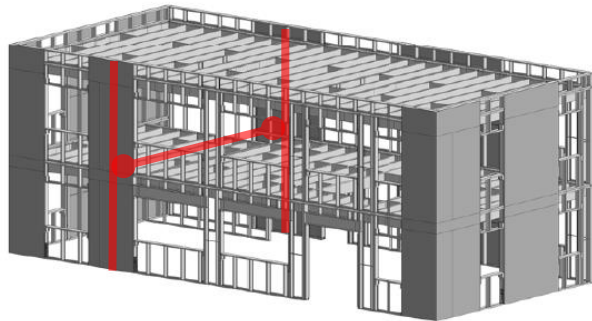
55 Initially, a general trend for the effect of incorporation of semi-rigid connections on the design of an  
56 archetype building, two-storey CFS-NEES building [2], is studied. The SFLS system is developed and  
57 assessed using finite element (FE) models featuring both the SCM and CCM designs. A stiffness  
58 estimation model is then developed for the semi-rigid SFLS connection and compared against the FE  
59 results.

## 60 **2. Two-storey CFS-NEES building frame assessment with semi-rigid connections**

### 61 *2.1 Joist-stud framed model specifications*

62 A two-storey single-span joist-stud framed model is adopted from the CFS-NEES building design  
63 (schematically shown in Fig. 1 (a)) [2]. The focus herein is on the design of the lower storey level joist  
64 and stud sections varying the joist-to-stud connection rotational stiffness ( $k$ ). Both the sequential  
65 and continuous construction methods (SCM and CCM) have been considered, with their frame  
66 models, respectively shown in Figs. 1 (b) and (c). Half-height studs were modelled for the CCM

67 configuration representing the inflection points of the studs. For the SCM configuration, a restraining  
 68 point is assumed at the half-height of the studs accounting for the bridging. Through-fastened to  
 69 floor sheathing condition is assumed for the design of the joists as laterally braced members. Both of  
 70 these boundary conditions for the joists and studs were defined as the design criteria within the  
 71 computational model. The span length of 6.6m and height of 2.7m are taken from the CFS-NEES  
 72 design narrative [2]. The flooring joists are laid down 600 mm on-centre, which are subjected to a  
 73 uniform distributed loading (UDL) of 3.5 kN/m<sup>2</sup> (LL: Live Load) and 1.0 kN/m<sup>2</sup> (DL: Dead Load),  
 74 adopted from the design narrative [2]. The upper storey roof loading is transferred to the lower  
 75 storey studs through the point loads of 2.0 kN (LL) and 3.0 kN (DL) as per [2].



(a) CFS-NEES two-storey building [2]

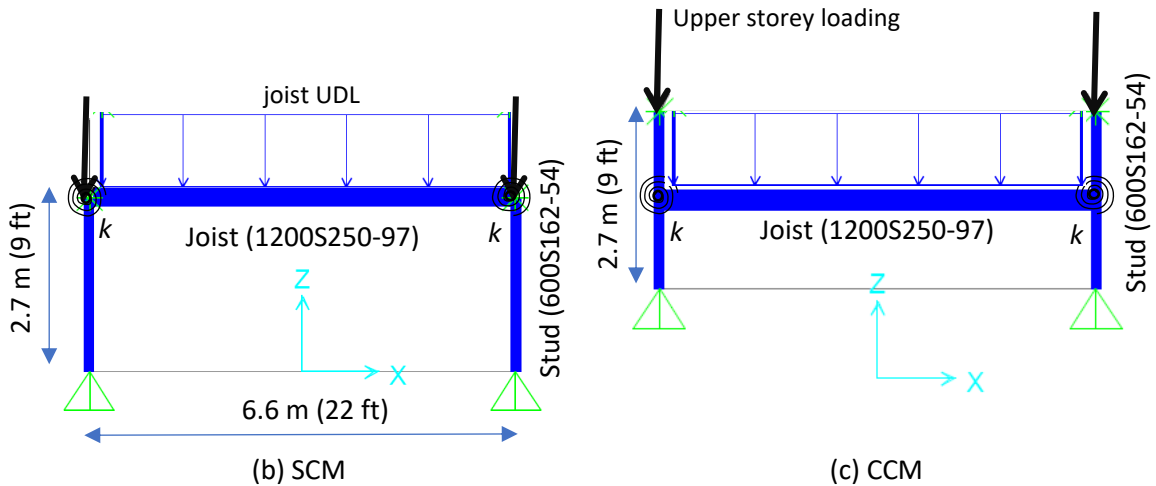


**Figure 1.** Lower storey joist-stud framed SCM and CCM configurations adopted from CFS-NEES two-storey building [2].

93 The 1200S250-97 joist and 600S162-54 stud lipped sections (with the web depths of 304 and 152  
 94 mm, flange widths of 64 and 41 mm and thicknesses of 2.5 and 1.4 mm, respectively), using the AISI  
 95 S240 [4] nomenclature, have been adopted from the CFS-NEES narrative [2], which were designed  
 96 based on the nominal yielding strength of 345 MPa and modulus of elasticity of 203,500 MPa. These  
 97 are considered herein as the benchmark designs for both the SCM and CCM joist-stud frames. An

98 imposed eccentricity of  $e = 76$  mm between the face of the stud wall to the centre line of the stud  
99 section was considered in the design process [2] to transfer the joist shear force to the wall studs.

100

## 101 *2.2 Joist-stud framed model results and discussions*

102 The joist-stud framed models have been analysed employing CSI SAP2000 [5] and designed based on  
103 AISI-S100-2016. Tables 1 and 2 list the designed joist and stud sections and their corresponding  
104 Demand-to-Capacity Ratios (DCRs) for SCM and CSM frames, respectively. These are related to a  
105 wide range of the connection rotational stiffness ( $k$ ) from a simply supported frame (the benchmark  
106 design) to a fully fixed frame. The joist design limit states include mid-span bending moment,  
107 denoted by  $M$ ; the bending moment and shear force combined effect at the joist end location,  
108 denoted by  $M+V$ ; and the mid-span deflection, limited to lesser of span length/240 for DL+LL or  
109 length/360 for LL [2], denoted by  $D$ . The stud is designed based on the combined bending moment  
110 and compression force, denoted by  $M+C$ . To minimise the variation of the joist and stud cross-  
111 sections, the overall dimension of the joist and stud sections were kept the same as those of the  
112 benchmark designs. In total three sets of joist and stud cross-sections have been designed  
113 corresponding to the three identified ranges of the connection rotational stiffnesses of  $k \leq 500$ ,  $500$   
114  $< k \leq 2000$  and  $k > 2000$  kN.m/rad (see Tables 1 and 2 for SCM and CCM, respectively). For better  
115 comparison, Fig. 2 illustrates the average trend of the DCRs for both the SCM and CCM designs.

116

117

**Table 1. SCM joist-stud framed design**

$k$ (kN.m/rad)	Joist section*	Joist DCR		Stud section*	Stud DCR
0 ( $e=76$ mm)	1200S250-97	0.76 ( $M$ )	0.92 ( $D$ )	600S162-54	0.73 ( $M+C$ )
103 ( $e=76$ mm)	1200S250-97	0.73 ( $M$ )	0.87 ( $D$ )	600S162-54	0.89 ( $M+C$ )
500 ( $e=0$ )	1200S250-97	0.72 ( $M$ )	0.85 ( $D$ )	600S162-54	1.01 ( $M+C$ )
1000 ( $e=0$ )	1200S250-97	0.69 ( $M$ )	0.80 ( $D$ )	600S162-68	0.91 ( $M+C$ )
2000 ( $e=0$ )	1200S250-97	0.68 ( $M$ )	0.78 ( $D$ )	600S162-68	0.97 ( $M+C$ )
3000 ( $e=0$ )	1200S250-68	1.06 ( $M$ )	0.94 ( $D$ )	600S162-97	0.91 ( $M+C$ )
5000 ( $e=0$ )	1200S250-68	1.05 ( $M$ )	0.93 ( $D$ )	600S162-97	0.93 ( $M+C$ )
10000 ( $e=0$ )	1200S250-68	1.04 ( $M$ )	0.92 ( $D$ )	600S162-97	0.95 ( $M+C$ )
Fully-Fixed ( $e=0$ )	1200S250-68	1.03 ( $M$ )	0.90 ( $D$ )	600S162-97	0.98 ( $M+C$ )

\*1200S250- joist and 600S162- stud lipped sections with the web depths of 304 and 152 mm and flange widths of 64 and 41 mm; the two-digit number after dash refers to the section thicknesses of 1.4 mm (54), 1.8 mm (68) and 2.5 mm (97).

118

**Table 2. CCM joist-stud framed design**

$k$ (kN.m/rad)	Joist section*	Joist DCR		Stud section*	Stud DCR
0 ( $e=76$ mm)	1200S250-97	0.75 ( $M$ )	0.92 ( $D$ )	600S162-54	0.62 ( $M+C$ )
103 ( $e=76$ mm)	1200S250-97	0.71 ( $M$ )	0.85 ( $D$ )	600S162-54	0.74 ( $M+C$ )
500 ( $e=0$ )	1200S250-97	0.65 ( $M$ )	0.76 ( $D$ )	600S162-54	0.92 ( $M+C$ )
1000 ( $e=0$ )	1200S250-68	0.94 ( $M$ )	0.85 ( $D$ )	600S162-68	0.92 ( $M+C$ )
2000 ( $e=0$ )	1200S250-68	0.87 ( $M+V$ )	0.76 ( $D$ )	600S162-68	1.02 ( $M+C$ )
3000 ( $e=0$ )	1200S250-68	0.96 ( $M+V$ )	0.66 ( $D$ )	600S162-97	0.77 ( $M+C$ )
5000 ( $e=0$ )	1200S250-68	1.00 ( $M+V$ )	0.62 ( $D$ )	600S162-97	0.80 ( $M+C$ )
10000 ( $e=0$ )	1200S250-68	1.03 ( $M+V$ )	0.59 ( $D$ )	600S162-97	0.82 ( $M+C$ )
Fully-Fixed ( $e=0$ )	1200S250-68	1.08 ( $M+V$ )	0.55 ( $D$ )	600S162-97	0.85 ( $M+C$ )

\*1200S250- joist and 600S162- stud lipped sections with the web depths of 304 and 152 mm and flange widths of 64 and 41 mm; the two-digit number after dash refers to the section thicknesses of 1.4 mm (54), 1.8 mm (68) and 2.5 mm (97).

119

120

121

122

123

124

125

126

127

128

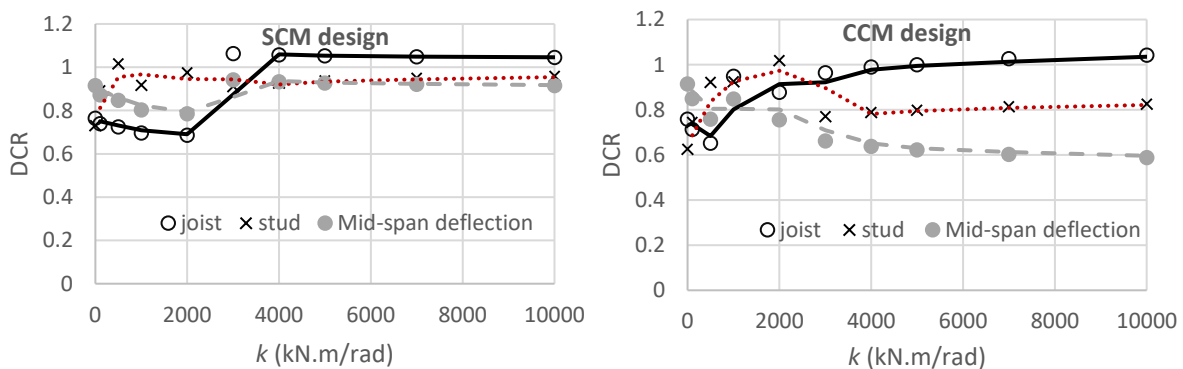


**Figure 2. Average trends for joist and stud DCRs for SCM and CCM designs.**

129 For the benchmark design with  $k=0$ , the joist deflection dominates the design with DCR ratio of 0.92  
130 (for both SCM and CCM designs) complying with the CFS-NEES design narrative [2]. The connection  
131 rotational stiffness of  $k=103$  kN.m/rad is adopted from the recently completed experiments for the  
132 ledger-framed floor-to-wall connections (test T5 reported in [3]). Compared with the benchmark  
133 design, the stud DCR is increased by 22% from 0.73 to 0.89 and dominates the SCM design, while the  
134 deflection DCR is reduced 5% from 0.92 to 0.87. For the CSM design, the stud DCR is also increased  
135 by 19% from 0.63 to 0.75. This indicates that even a low level of connection rotational stiffness,  
136 which is generally being ignored in the joist-stud framed design [2], can noticeably affect the overall  
137 design towards an unconservative side. The unconservative design might arise when the initial DCR  
138 is close to unity, and the additional demands due to partial fixity would push the stud DCR above  
139 unity, thus requiring a larger stud section. This effect can result in unexpected failures in wall studs  
140 under extreme loading conditions (i.e. wind or seismic), even compromising the gravity loading  
141 system.

142

143 For joist-stud framed designs with higher connection rotational stiffness ( $k=500$  kN.m/rad and  
144 beyond), the connection eccentricity of  $e=0$  is assumed consistent with the details of the SFLS semi-  
145 rigid connections discussed in the following sections. Variation of the connection rotational stiffness  
146 from simply supported (benchmark design) to fully fixed conditions has resulted in the joist and stud  
147 sections, with the same overall dimensions, ranging three sets of thicknesses of 97-54, 97-68, and  
148 68-97 mils for SCM design, and 97-54, 68-68, and 68-97 mils for CSM design. The section thicknesses  
149 of 54, 68 and 97 in mils unit are respectively equivalent to 1.4, 1.8 and 2.5 mm in SI units. The overall  
150 trend is shifting from a heavier joist section (having 97 mils thickness) governed by deflection  
151 (deemed undesirable) for the lower  $k$  values towards a 28% lighter joist section (having 68 mils  
152 thickness) governed by strength (deemed desirable) for the higher  $k$  values. This is more noticeable  
153 for the CCM design and has been achieved at  $k=1000$  kN.m/rad, while  $k=3000$  kN.m/rad is the  
154 minimum stiffness level for the joists to be dominated by strength in the SCM design. This is  
155 attributed to the higher CCM joist-stud framed stiffness compared with that of the SCM design.  
156 Heavier stud sections (having 68 or 97 mils thicknesses) are, however, required for both the SCM  
157 and CCM designs due to the larger bending moments imposed to the studs at higher  $k$  values.

158

159 In general, the CCM design can provide a more uniform joist bending moment distribution, that can  
160 be observed in Fig. 3. The figure shows a smaller gap between the averaged trends of the mid-span  
161 and end moments (normalised by the mid-span  $M$  for the benchmark design with  $k=0$ ) for the CCM

162 design compared with that of the SCM design. The more economical design could be achieved for  $k$   
163 values in the range of  $500 < k \leq 2000$  kN.m/rad with a lighter joist section having 68 mils thickness  
164 for CCM compared with 97 mils for SCM designs. However, the higher CCM joist end bending  
165 moment values (shown in Fig. 3) caused the combined moment and shear effect ( $M+V$ ) to govern in  
166 the design with  $k= 2000$  kN.m/rad and beyond (with the high DCRs of 0.87 and above, referring to  
167 Table 3). This resulted in the same joist section of 1200S250-68 for both SCM and CCM designs with  
168  $k= 3000$  kN.m/rad and beyond, governed by  $M$  and  $M+V$ , respectively.

169

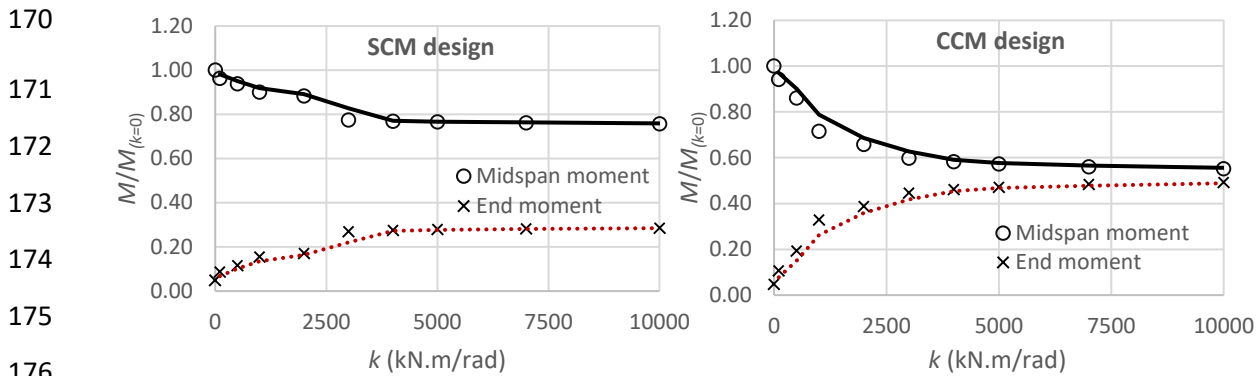


**Figure 3.** Averaged trend for joist mid-span and end bending moments for SCM and CCM designs.

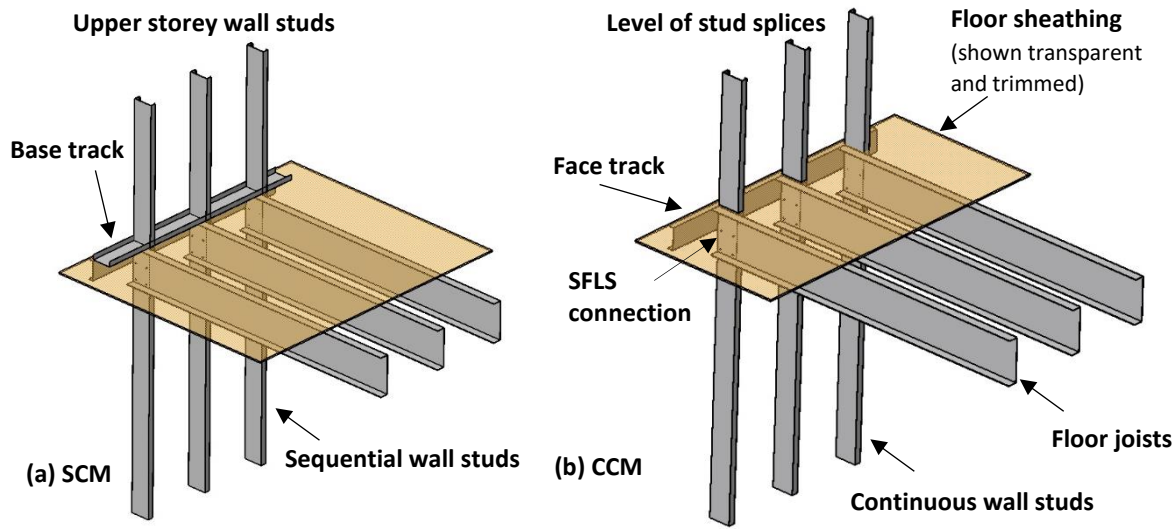
### 3. Side-framed lightweight steel system with semi-rigid connections

Within this section, a side-framed lightweight steel (SFLS) flooring joist-to walling stud semi-rigid connection has been detailed and assessed under distributed gravity loading. In this system, the flooring joists are attached to the side of the walling studs through a planar screw connection pattern, schematically shown in Figs. 4 (a) and (b) for SCM and CCM, respectively. The imposed eccentricity within the recently tested ledger-framed connections [3], which causes unavoidable out-of-plane actions and local failures (which may end up in a larger stud thickness), would, therefore, be eliminated within the SFLS type of connection. Furthermore, compared with the ledger-framed systems, the ledger beams and the joist-to-ledger clip angle connections are eliminated, which together with the lighter joist sections using semi-rigid connections (see Section 2) can potentially lead to a more efficient and economical LSF system.

When the joists are not continuous (for the case of alternate joist orientation or external walls), a face-track (shown in Figs 4 (a) and (b)) could run at the opposite side of the wall and is attached to the wall studs (in lieu of the conventional top tracks). The face-track provides a lateral restraining effect for the studs and supports the floor and wall sheathings. The in-plane strap braces, if present, can be connected to the face of the studs below or above the joist levels with no interference with the face tracks which are levelled with the joist top flanges and are typically shallower than the joists. When the joists are extended to the opposite side of the walls, the face tracks can be placed in segments between the studs. Figs. 4(a) and (b) also shows a wood-based sheathing attached to the top of the joists which can be extended to the opposite side of the walls for the case of alternate joist orientation.



202  
203  
204  
205  
206  
207  
208  
209  
210  
211  
212  
213



214 **Figure 4.** Schematic drawing of the SFLS floor-to-wall connection system for both (a) SCM and (b) CCM.

215  
216  
217  
218  
219  
220  
221

A detailed finite element analysis using ABAQUS [6] has been employed to model the SFLS flooring joist-to-walling stud semi-rigid connections. The main features of the finite element (FE) models have been firstly validated against a tested configuration of the ledger-framed floor-to-wall connections [3]. The validated FE models are then used to assess the SFLS connections based on a range of joist and stud sections taken from the results of the SCM and CCM joist-stud framed designs presented in the previous section.

222  
223

### 3.1 SFLS FE modelling specifications

224  
225  
226  
227  
228  
229  
230  
231  
232

Figs. 5 (a) and 5 (b) show typical SFLS FE models for both the SCM and CCM configurations, respectively, comprising a double joisted sheathed floor connected to the wall studs. The overall joist and stud dimensions and the floor UDL and the upper storey loading are the same as those of the design given in Section 1 (adopted from the CFS-NEES project [2]). A hinge boundary condition is applied at the base section of the studs to the reference point RP-1, shown in Figs. 5(a) and 5(b), to which all the degrees of freedom of that section are coupled. Mid-height bridging restraint is applied at RP-2 in the SCM configuration coupled to the stud sections at that level. The symmetric boundary condition is applied to the mid-span section of the joists at RP-3. The upper storey loading is applied through RP-4 coupled to the studs at the top section with free translation and rotation, respectively

233 in vertical (Y-direction) and about X-direction. The lateral supports, representing blocking restraints,  
234 are applied to the joists at the mid-span and the connection end sections.

235

236 A bi-linear stress-strain curve has been utilised for the steel with the nominal yielding strength and  
237 modulus of elasticity same as those used in the frame model (see Section 2, based on CFS-NEES  
238 narrative [2]) and the strain hardening second modulus ratio of  $E / E_s = 0.01$ . The joists are connected  
239 to the side face of the studs using self-drilling #12 screw connections with 5.4 mm thread diameter.  
240 An OSB sheathing, with a modulus of elasticity of 699 MPa [7], is attached to the top of the joists and  
241 the face track with the same #12 screws. The screw connections are modelled using Point-based  
242 Cartesian Fasteners, available in the Abaqus library, with the radius of influence equals to the thread  
243 diameter. This modelling technique has successfully been used previously in FE modelling of CFS  
244 connections [8]. Quad-linear load-deformation backbone curves, shown in Fig. 6, have been adopted  
245 from [7] for the steel-to-steel and the OSB-to-steel screw fasteners.

246

247 Nonlinear analysis has been performed using the arc-length algorithm, which takes the load  
248 magnitude as unknown and solves simultaneously for loads and displacements [6]. This method has  
249 been successfully employed in previous studies [8-10] to capture local buckling instability and  
250 incorporation of material and geometrical nonlinearity of structures. The second order S8R shell  
251 element was employed for all the steel sections having 8 nodes, each with 6 translational and  
252 rotational degrees of freedom and reduced integration. A mesh size of 10 mm × 10 mm was chosen,  
253 which shown [8-9] to capture the load-deformation response of CFS connections with high accuracy.  
254 For OSB sheathing, S4R shell type with a coarser mesh size of 50 mm × 50 mm have been adopted  
255 since the failure behaviour of OSB is not the intention of this research. Hard contact with Penalty  
256 formulation [6] has been applied between the OSB and the top surfaces of the joists and the face  
257 track. The same contact type has also been applied within the connection region between the  
258 surfaces of the joists, studs and the face track.

259

260

261

262

263

264

265  
266  
267  
268  
269  
270  
271  
272  
273  
274  
275  
276  
277  
278  
279  
280  
281

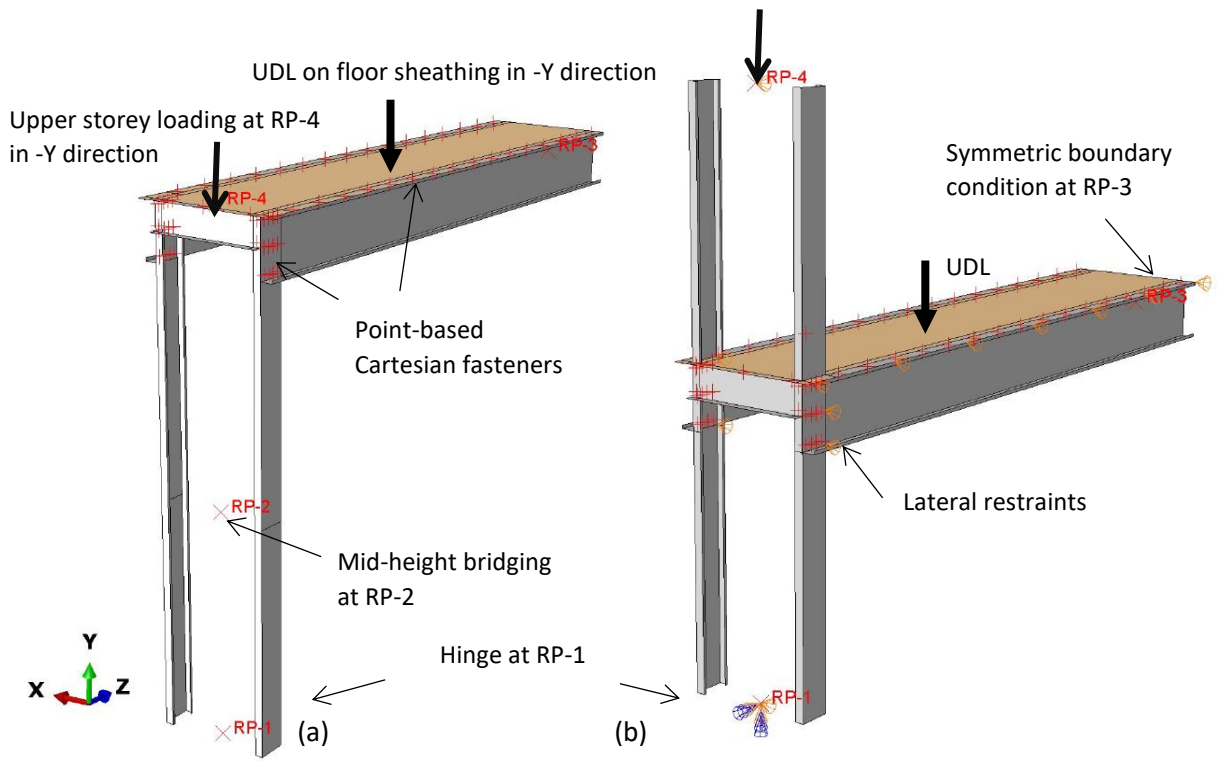


**Figure 5.** Overall view for (a) SCM and (b) CCM FE models: Boundary conditions, loading and fasteners.

282  
 283  
 284  
 285  
 286  
 287  
 288  
 289  
 290  
 291  
 292  
 293  
 294  
 295  
 296  
 297  
 298  
 299  
 300  
 301  
 302  
 303  
 304  
 305  
 306  
 307  
 308  
 309  
 310  
 311  
 312

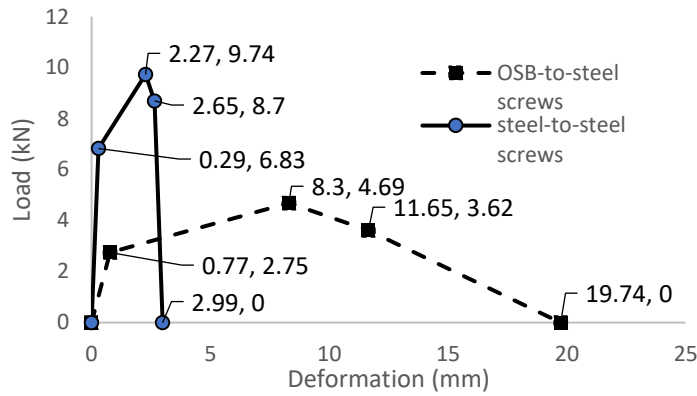


**Figure 6.** Load-deformation backbone curve for steel-to-steel and OSB-to-steel #12 self-drilling screws [7].

### 3.2 FE validation

Fig. 7 (a) shows the set up for the tests on ledger-framed connections conducted at Johns Hopkins University reported in [3]. The test specimens consist of a single 1575 mm length joist connected to a ledger track through a 38 × 38 × 1.4 mm clip angle between two 813 mm height supporting studs. The studs were supported on a test rig placed at 600 mm apart and capped with a top track. The joist, stud, ledger and top track sections were 1200S250-97, 600S162-54, 1200T200-97 and 600T162-54 respectively, all using a nominal 345 MPa yield stress, while an OSB sheathing attached to the joist flange and the top track web. All the connections employed Simpson self-drilling #10 screws with 4.7 mm thread diameter. The joint web was connected to the ledger web using four screws at each leg of the clip angle. The top and bottom flanges of the joist were connected to the ledger flanges by a single screw, while the ledger itself was connected to the stud flanges by seven screws.

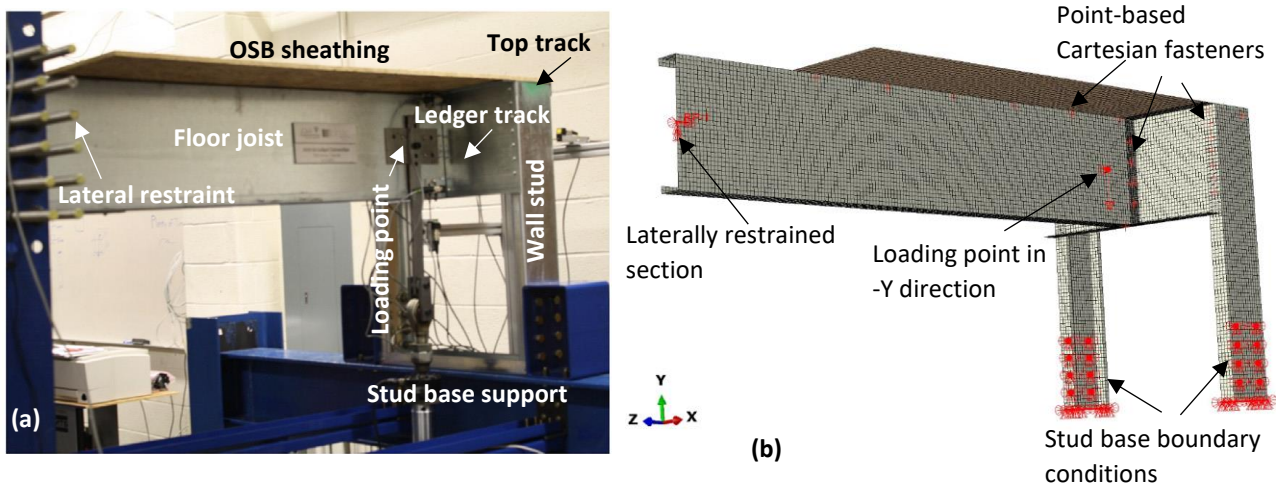
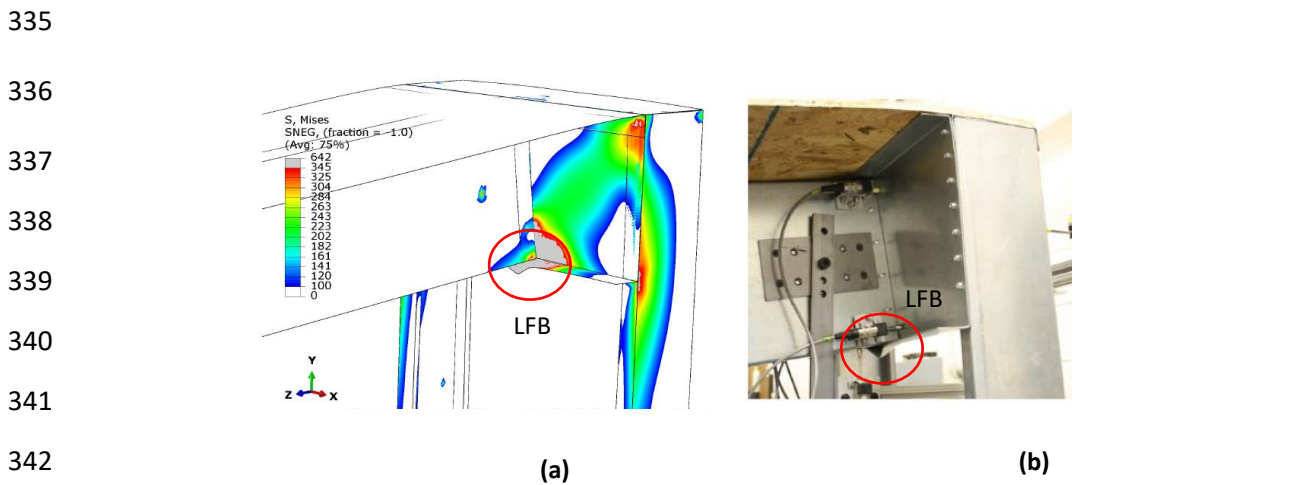


**Figure 7.** (a) Leger-framed connection tests [3] and (b) FE model for specimen T4.

313 Fig. 7(b) shows the FE model for the control test specimen (namely T4 in [3]) with the joist  
 314 positioned at the middle length between the studs and the loading applied at 127 mm from the face  
 315 of the ledger. All the modelling specifications, including the element type and sizes, contact  
 316 behaviour, connection fasteners and analysis algorithm were the same as the SFLS model above.  
 317 Similarly, the load-deformation behaviour of #10 screws for all the connection fasteners was  
 318 adopted from the extensive single-lap tests reported in [7] using linear interpolation for the  
 319 unavailable 97-54 and 54-54 steel plies. Also, the fastener pull-out load-deformation behaviour was  
 320 taken from the test results recently published in [11]. It should be noted that the fastener pull-out  
 321 failure is a critical limit state for the ledger-framed connections due to the out-of-plane nature of  
 322 load transferring mechanism between the joists, ledger and studs. In SFLS connections, however, the  
 323 shear behaviour is expected to be the dominant limit state (which is discussed later herein) within  
 324 the proposed planar type of connection.

325  
 326 Fig. 8 (a) shows the ledger flange buckling (LFB) captured by the FE model which occurred in the T4  
 327 test, as can be observed in Fig. 8 (b), as the dominant failure limit state. Further, the overall trend of  
 328 the moment-rotation behaviour estimated by FE analysis, as shown in Fig. 9, matches reasonably  
 329 well with that of the test. The peak strength and initial stiffness predictions by the FE analysis are  
 330 within 5% and 10% of those of the test, respectively. These relatively small differences could be due  
 331 to the deviations of the load-deformation behaviour of the fasteners in the tests and those  
 332 incorporated in the FE taken from [7] and [11]. Furthermore, the contact behaviour between various  
 333 steel-to-steel and OSB-to-steel surfaces in the ledger-framed connections might have deviated from  
 334 that assumed in the FE simulations.



343 **Figure 8.** (a) FE prediction and (b) T4 test ledger flange buckling for ledger-framed connection.

344

345  
346  
347  
348  
349  
350  
351  
352  
353  
354  
355  
356  
357  
358  
359  
360  
361  
362  
363  
364  
365  
366  
367  
368  
369  
370  
371  
372

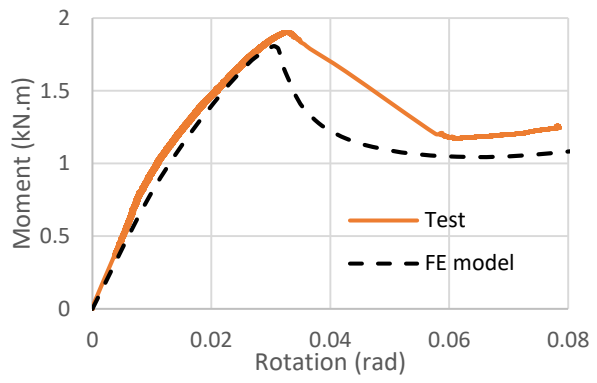
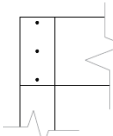
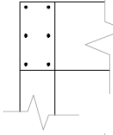
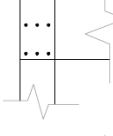



Figure 9. Moment-rotation behaviour of the FE and T4 test ledger-framed connection.

### 3.3 SFLS FE results and discussions

FE analysis was conducted for three sets of the joist and stud sections adopted from the joist-stud framed models in Section 2, corresponding to ranges of connection rotational stiffness within  $k \leq 500$ ,  $500 < k \leq 2000$  and  $k > 2000$  kN.m/rad (see Tables 1 and 2 for SCM and CCM, respectively). A semi-rigid SFLS connection has been designed using one to four vertical lines of screws for the identified ranges of connection rotational stiffness, each line having three #12 screws at the middle, top and bottom height of the connection (shown in Table 3). It should be noted that the choice of one to four vertical lines of screws is for consistency and comparison purposes and does not necessarily represent the optimum arrangements with the minimum number of screws. The FE models (listed in Table 3) are labelled with the start letter of S or C standing for the relevant construction method (SCM or CCM), followed by a 4-digit number representing the thicknesses of the joist and the stud sections of 1.4 mm (54), 1.8 mm (68) and 2.5 mm (97) ended by a single-digit number indicating the number of vertical lines of screws (1 to 4). In addition, two benchmark models of S9754-0 and C9754-0 were designed with one screw at the middle height of the SFLS connection corresponding to the  $k = 0$  connection rotational stiffness in the joist-stud framed models in Section 2 adopted from CFS-NEES [2] with simply supported shear connection. The shear capacity of a single #12 screw connection is sufficient to transfer the design shear force based on DL+LL specified in Section 2.

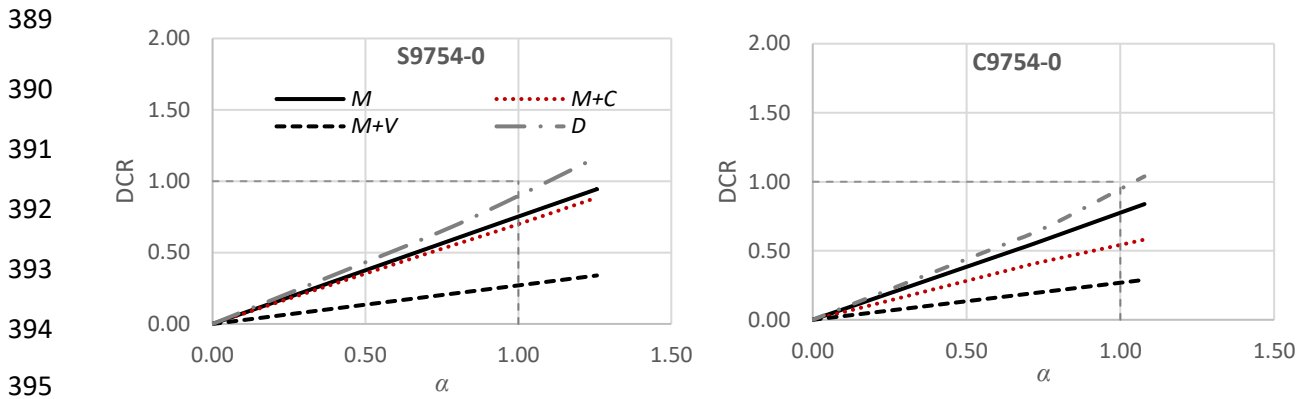
**Table 3. SFLS FE models.**

Label*	Construction	Joist section	Stud section	Vertical screw lines
S9754-1,2,3 or 4	SCM	1200S250-97	600S162-54	 1 line of three #12 @ middle length of the connection
C9754-1,2,3 or 4	CCM	1200S250-97	600S162-54	
S6868-1,2,3 or 4	SCM	1200S250-68	600S162-68	 2 lines of three #12@ 26mm from side edges of the connection
C6868-1,2,3 or 4	CCM	1200S250-68	600S162-68	
S9768-1,2,3 or 4	SCM	1200S250-97	600S162-68	 3 lines of three #12 @ equally distanced
C9768-1,2,3 or 4	CCM	1200S250-97	600S162-68	
S6897-1,2,3 or 4	SCM	1200S250-68	600S162-97	 4 lines of three #12 @ equally distanced
C6897-1,2,3 or 4	CCM	1200S250-68	600S162-97	

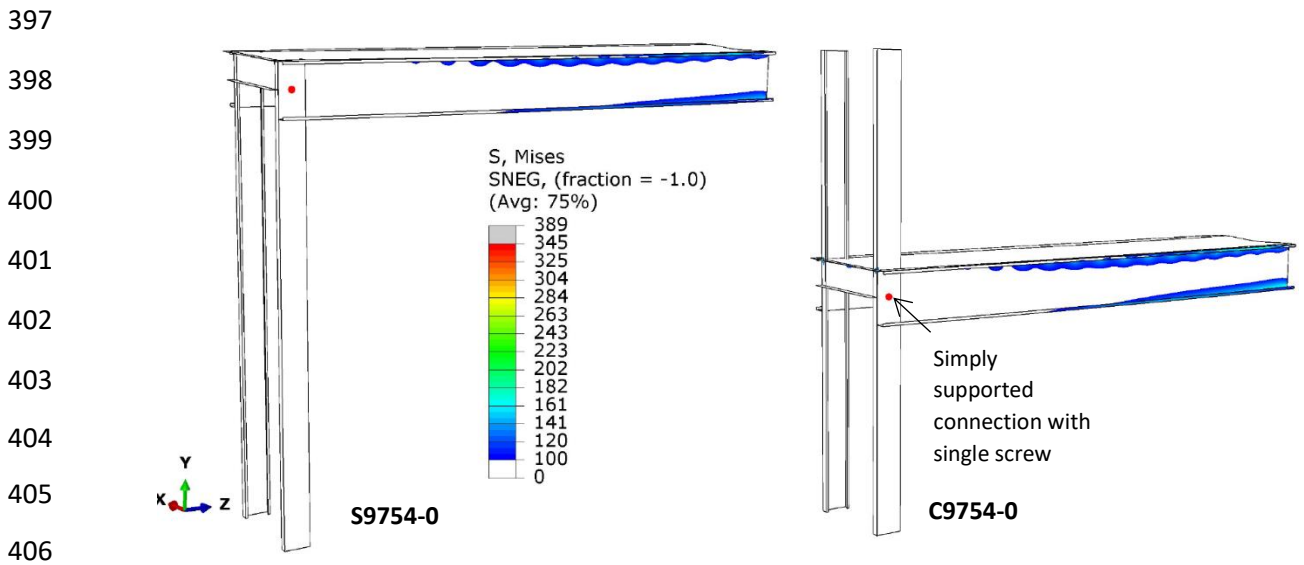
\*Definition of the labels: letters S and C stand for SCM and CCM; 4-digit number (9754, 6868, 6897 and 9768) represent the thickness of joist and stud sections: 1.4 mm (54), 1.8 mm (68) and 2.5 mm (97); single-digit number after dash refers to the vertical lines of #12 screws.

### 373 3.3.1 Benchmark FE designs

374 Fig. 10 shows the DCRs for the benchmark models varying with the load ratio ( $\alpha$ ). The DCRs  
375 correspond to those limit states identified in the joist-stud framed designs (in Section 2) with the  
376 same labels of  $M$ ,  $M+V$  and  $D$  for the joists and  $M+C$  for the studs. The load ratio,  $\alpha$ , is the total  
377 applied floor and upper storey loads divided by the total design DL+LL loads with the same  
378 magnitudes as those utilised for the joist-stud framed designs in Section 2 which were adopted from  
379 CFS-NEES project [2]. As predicted in Section 2 for the frames with  $k = 0$ , the joist mid-span  
380 deflection limit state (shown by  $D$  in Fig. 10) dominates the design with DCR ratio close to unity at  
381  $\alpha = 1$ . Shaded areas in Fig. 11 show the corresponding von-Mises stress distributions of the benchmark  
382 designs. For a better understanding of the most critical portions, the stress contour is set to display  
383 those areas greater than 100 MPa. As expected, the results are identical for both the S9754-0 and  
384 C9754-0 designs. By increasing the stress limit to 206 MPa (which is the level of stress calculated  
385 from the nominal yielding stress of 345 MPa divided by the design safety factor of 1.67), all the  
386 shaded areas are diminished. The results indicate an underutilised design strength of the joist and  
387 stud sections being dominated by the joist mid-span deflection and floor vibration for the simply  
388 supported joist-stud framed models, reflecting the CFS-NEES design [2].



396 **Figure 10.** Variation of DCRs with  $\alpha$  for  $M$ ,  $M+V$ ,  $M+C$ , and  $D$  limit states for S9754-0 and C9754-0 designs.



407 **Figure 11.** Von-Mises stress contour greater than 100 MPa for S9754-0 and C9754-0 designs at  $\alpha = 1$ .

409 **3.3.2 Variation of connection rotational stiffness**

410 Fig. 12 shows different levels of connection rotational stiffness varied with the load ratio of  $\alpha = 0$  to  
 411 2, corresponding to various connection configurations having sets of one to four vertical screw lines  
 412 (labelled by 1-4 shown by different line thicknesses). Also, the benchmark design using single screw  
 413 connection (labelled by zero) is shown by dashed lines with connection rotational stiffness close to  
 414 zero, mainly indicating the ignorable composite action between the joist and OSB. The connection  
 415 rotational stiffness is derived by dividing the connection bending moment by the connection  
 416 rotation; whereas, the connection rotation is calculated by subtracting the stud contribution from  
 417 the joist rotation at the connection centroid. As can be seen, the connection rotational stiffness  
 418 slightly degrades by increasing the load ratio followed by a sharp degradation which is more  
 419 noticeable in the CCM connections which also produce slightly lower initial connection rotational  
 420 stiffness compared with that of the SCM connections. The initial degradation can be attributed to



421 the local connection effects and diminishing of relatively small composite action between the joist  
422 and the flooring OSB due to the yielding of OSB-to-steel screws at the connection region. The  
423 afterwards sharp degradation occurs due to the yielding of the joist-to-stud connection screws,  
424 which is more critical for the connections with a lower number of screws for the CCM connections. A  
425 more detailed discussion is presented under section 3.3.5, where the screw forces of SCM and CCM  
426 connections are given.

427

428 Based on the connection rotational stiffness level at  $\alpha = 1$ , using one to four vertical lines of three  
429 #12 screws falls within the ranges of  $k \leq 500$ ,  $500 < k \leq 2000$  and  $k > 2000$  kN.m/rad specified in  
430 Tables 1 and 2 corresponding to the 97-54, 97-68, 68-68 and 68-97 joist-stud SCM and CCM designs.  
431 The FE results for each of the connection configurations are presented in the following subsections.

432

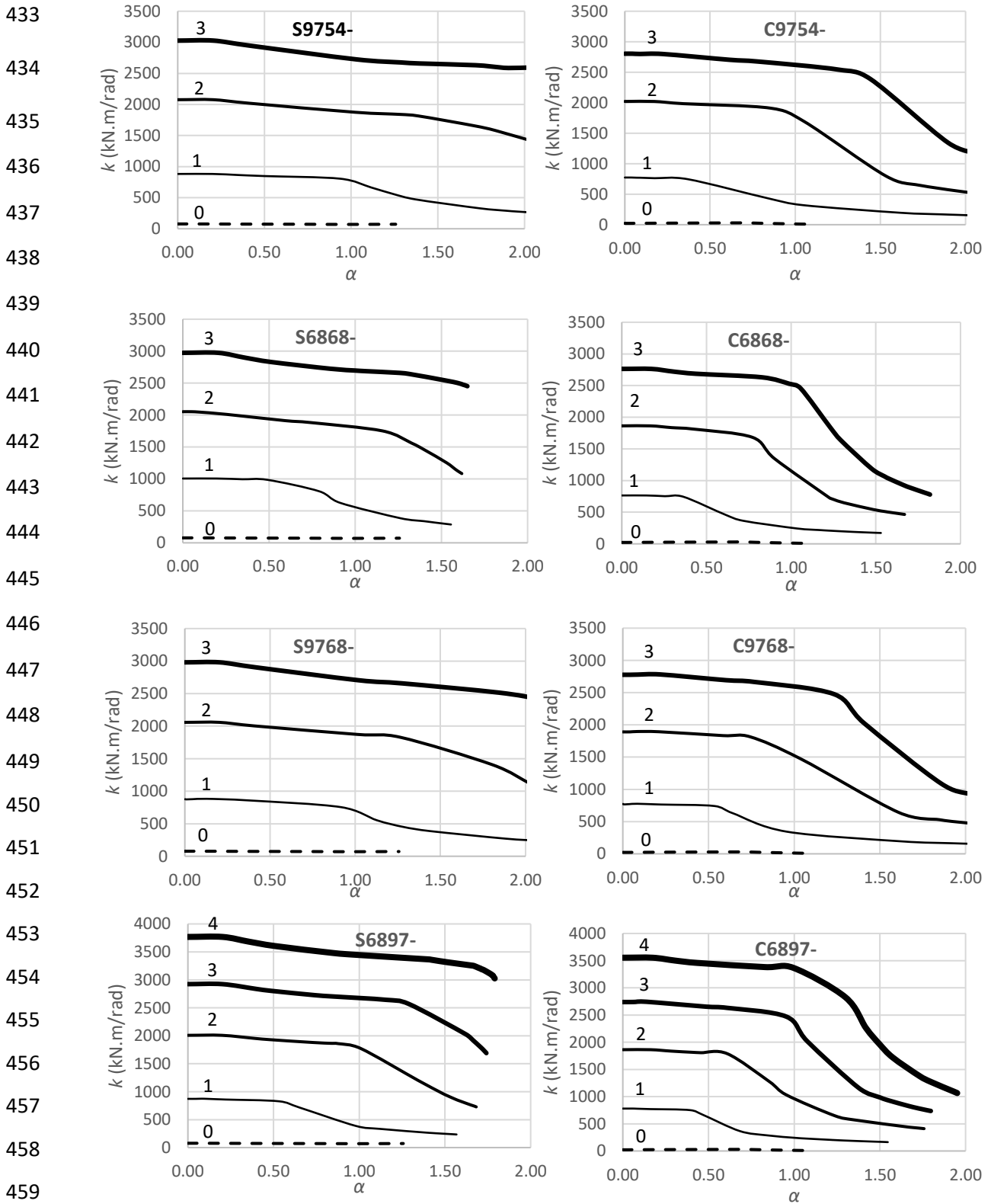


Figure 12. Variation of the connection rotational stiffness,  $k$ , with the load ratio,  $\alpha$ , for connections with one to four vertical lines of screws and the benchmark connection.

465 3.3.3 Overall designs

466 Tables 4 and 5 summarises the DCRs for all the SFLS connections within the whole range of the  
 467 identified connection rotational stiffness at  $\alpha = 1$ , for SCM and CCM respectively. Three bands of  
 468 DCRs have been specified indicating the design status and the material utilisation of the joists and  
 469 studs. These are:  $DCR > 1$ ,  $0.8 \leq DCR \leq 1$  and  $DCR < 0.8$ , respectively refer to failed (denoted by F),  
 470 efficient/economical design (denoted by E) and oversized (denoted by O) DCRs. Furthermore,  
 471 the status of the screw shear forces in respect to the yielding force level at  $\alpha = 1$ , identified as one of  
 472 the failure limit states, has been added being acceptable or undesirable (denoted by A or U). The  
 473 successful designs, matching those presented in Section 2, are highlighted by grey colour, whilst the  
 474 rest deemed unsuccessful designs due to the failed limit states or undesirable level of the screw  
 475 shear forces. The results for successful designs as well as some examples of unsuccessful designs is  
 476 discussed in more details in the following subsections.

477

**Table 4. DCRs for SFLS SCM connections.**

Connection label	$k$ at $\alpha = 1$ (kN.m/rad)	Joist			Stud	Screw shear forces
		$M$	$M+V$	$D$	$M+C$	
S9754-0	0	O	O	E	O	<b>U</b>
S9754-1	500-2000	O	O	O	<b>F</b>	<b>U</b>
S9754-2	500-2000	O	O	O	<b>F</b>	A
S9754-3	>2000	O	O	O	<b>F</b>	A
S6868-1	500-2000	<b>F</b>	E	<b>F</b>	<b>F</b>	<b>U</b>
S6868-2	500-2000	<b>F</b>	E	E	<b>F</b>	A
S6868-3	>2000	<b>F</b>	E	E	<b>F</b>	A
S9768-1	500-2000	O	O	O	E	<b>U</b>
S9768-2	500-2000	O	O	O	E	A
S9768-3	>2000	O	O	O	E	A
S6897-1	$\leq 500$	<b>F</b>	E	<b>F</b>	O	<b>U</b>
S6897-2	500-2000	<b>F</b>	E	E	E	A
S6897-3	>2000	<b>F</b>	E	E	E	A
<b>S6897-4</b>	<b>&gt;2000</b>	<b>E</b>	<b>E</b>	<b>E</b>	<b>E</b>	<b>A</b>

478 Joist and stud design status: Failed (F), Efficient/economical (E) & Oversized (O).

479 Screw design status: Acceptable (A) & Undesirable (U).

480

**Table 5. DCRs for SFLS CCM connections.**

Connection label	$k$ at $\alpha = 1$ (kN.m/rad)	Joist			Stud	Screw shear forces
		$M$	$M+V$	$D$	$M+C$	
C9754-0	0	O	O	E	O	<b>U</b>
C9754-1	$\leq 500$	O	O	O	E	<b>U</b>
C9754-2	500-2000	O	O	O	<b>F</b>	<b>U</b>
C9754-3	$>2000$	O	O	O	<b>F</b>	A
C6868-1	$\leq 500$	<b>F</b>	E	<b>F</b>	O	<b>U</b>
C6868-2	500-2000	E	E	E	E	<b>U</b>
<b>C6868-3</b>	<b><math>&gt;2000</math></b>	<b>E</b>	<b>E</b>	<b>O</b>	<b>E</b>	<b>A</b>
C9768-1	$\leq 500$	O	O	O	O	<b>U</b>
C9768-2	500-2000	O	O	O	E	<b>U</b>
C9768-3	$>2000$	O	O	O	E	A
C6897-1	$\leq 500$	<b>F</b>	E	<b>F</b>	O	<b>U</b>
C6897-2	500-2000	E	E	E	O	<b>U</b>
C6897-3	$>2000$	E	E	O	O	A
<b>C6897-4</b>	<b><math>&gt;2000</math></b>	<b>E</b>	<b>E</b>	<b>O</b>	<b>E</b>	<b>A</b>

481 Joist and stud design status: Failed (F), Efficient/economical (E) & Overdesigned (O).

482 Screw design status: Acceptable (A) & Undesirable (U).

483

#### 484 3.3.4 Detailed designs for connections with one vertical line of three #12 screws

485 Fig. 13 shows the DCRs for the  $M$ ,  $M+V$ ,  $D$  and  $M+C$  joist and stud limit states varied with the load  
486 ratio,  $\alpha$ , for S9754-1 and C9754-1 models. At  $\alpha = 1$  for S9754-1, the DCR for stud  $M+C$  exceed the  
487 unity and may not be acceptable, while all the DCRs for C9754-1 are below one. These agree with  
488 the SCM, and CCM joist-stud framed designs with  $k = 500$  kN.m/rad in Tables 1 and 2, respectively.  
489 Another limit state that needs to be considered in the design is the shear failure of the screwed  
490 connections. Fig. 14 shows the screw shear forces ( $P_s$ ) derived for the C9754-1 joist-to-stud fasteners  
491 normalised by the yielding load ( $P_{ny}$ ) of 6.83 kN in Fig. 6. As can be seen, the top and bottom screws  
492 (shown by solid lines) reached the yielding force level at a loading ratio,  $\alpha$ , less than unity. This is  
493 assumed herein as an undesirable limit state due to the residual deformation which could potentially  
494 occur under service loads over the lifetime of the structure. Therefore, the C9754-1 design with a  
495 single line of three #12 screws is also deemed unacceptable for the range of  $k \leq 500$  kN.m/rad.

496

497

498

499

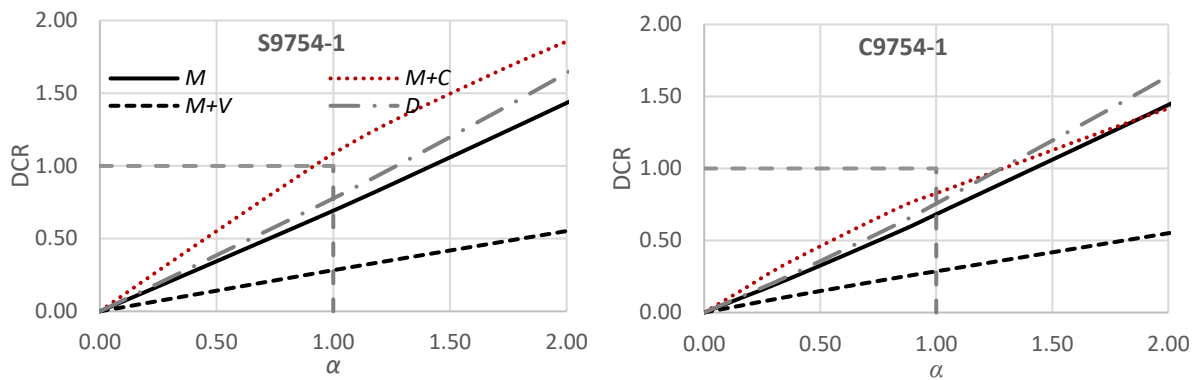
500

501

502

503

504



505 **Figure 13.** Variation of DCRs with  $\alpha$  for  $M$ ,  $M+V$ ,  $M+C$  and  $d$  limit states for S9754-1 and C9754-1 designs.

506

507

508

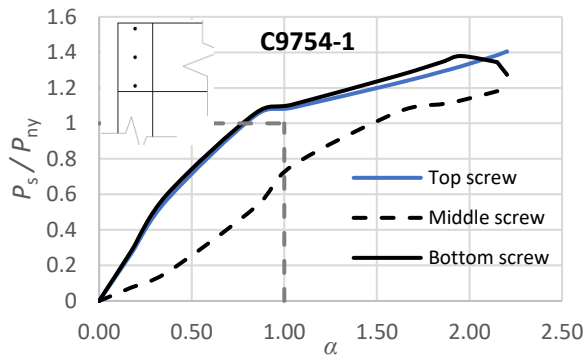
509

510

511

512

513



514 **Figure 14.** Variation of screw shear forces with  $\alpha$  for C9754-1 design.

515

516 **3.3.5 Detailed designs for connections with two to four vertical lines of three #12 screws**

517 Fig. 15 shows the variation of DCRs with  $\alpha$  for S9768-2& 3, C6868-2& 3, S6897-4 and C6897-4

518 designs chosen from Tables 4 and 5 with satisfactory joist and stud design limit states. As can be

519 noticed, the SCM S9768-2& 3 designs are governed by the stud  $M+C$  limit state with the DCR ratio

520 close to unity, whilst the joists are designed conservatively. By increasing the vertical screw lines to

521 4, a more economic SCM design can be achieved with all the limit states being dominant in the

522 S6897-4 design, thus more efficient design (highlighted in bold in Table 4). On the other hand, the

523 CCM designs led to a more economic joist and stud DCRs reasonably close to unity for all the C6868-

524 2, 3 and C6897-4 design cases. These results are consistent with those of the joist-stud framed

525 designs presented in Section 2. As an example of failed/unacceptable designs for the ranges within

526  $500 < k \leq 2000$  and  $k > 2000$  kN.m/rad, Fig. 15 also shows the DCRs of the S6868-2& 3 models for

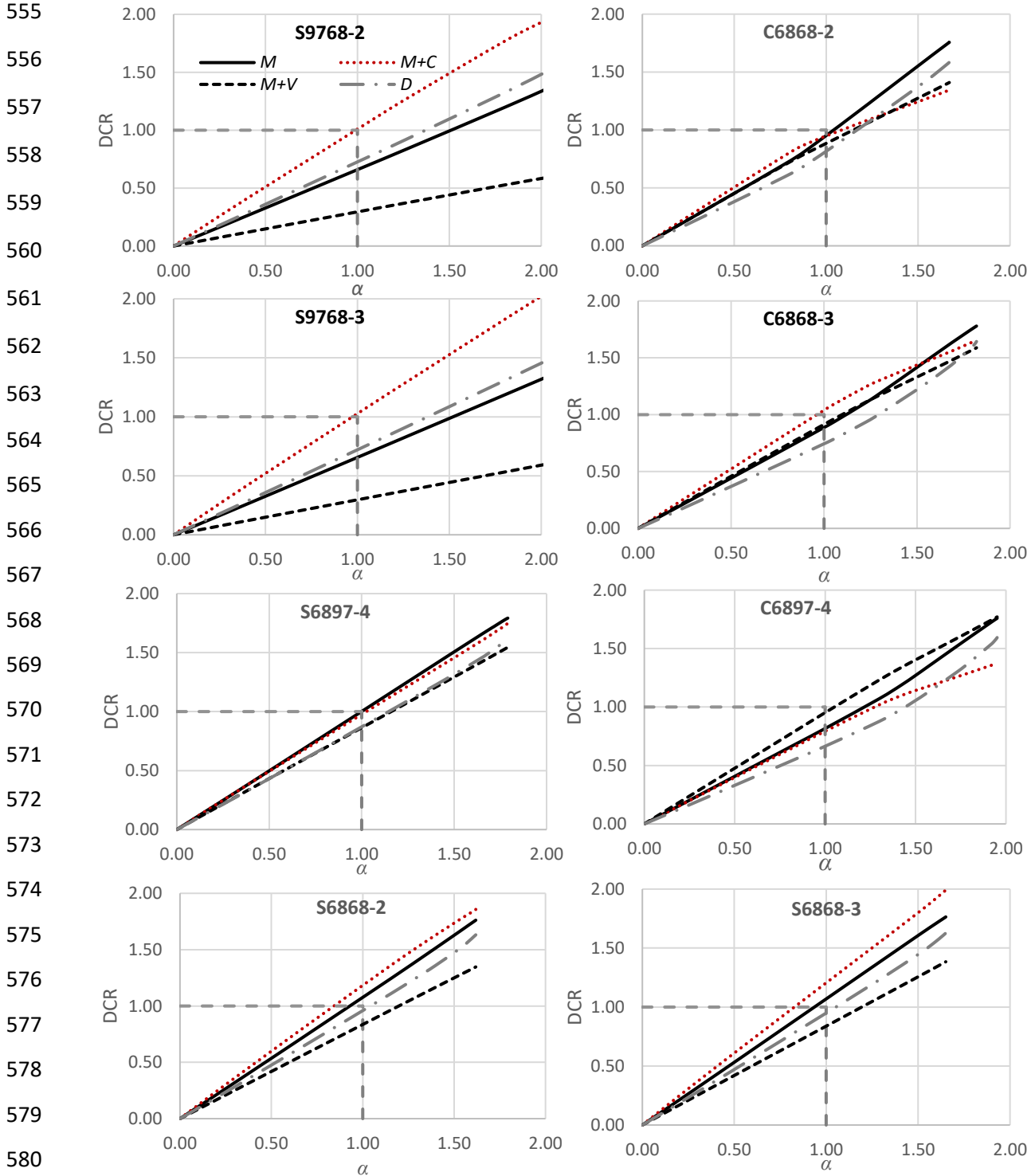
527 which the joist  $M$  and the stud  $M+C$  are both greater than unity at  $\alpha = 1$ . This design is consistent

528 with the joist-stud framed design (in Section 2) which resulted in the heavier set of 97-68 joist and  
529 stud sections rather than the more economical 68-68 sections (like the CCM design).

530 Fig. 16 shows the normalised screw shear forces for the top, middle and bottom rows of screws of  
531 the S9768-2& 3, C6868-2& 3, S6897-4 and C6897-4 designs. These curves indicate an acceptable  
532 level of shear forces being lower than  $P_{ny}$  at  $\alpha = 1$  for all the designs, except C6868-2 for which the  
533 shear forces of the top and bottom rows of screws reach  $P_{ny}$  at around  $\alpha = 0.8$ . The CCM designs, in  
534 general, led to higher screw shear forces than those of the corresponding SCM designs. This is due to  
535 the higher stud stiffness in the CCM designs, which led to lower stud rotation and as a result shifting  
536 the deformation demand to the connection. This means a higher CCM connection rotation at a  
537 certain load compared with that of the SCM connection. The higher deformation demand in the CCM  
538 connections than the SCM connections results in a generally slightly lower connection rotational  
539 stiffness and an earlier yielding in the CCM screws. This explains the more noticeable sharp  
540 degradation of the CCM connection rotational stiffness (observed in Fig. 12) as mentioned above.  
541 This may also lead to a higher number of screws for the CCM connections compared with that of the  
542 SCM connections to ensure elastic behaviour at  $\alpha = 1$  as a desirable design requirement.

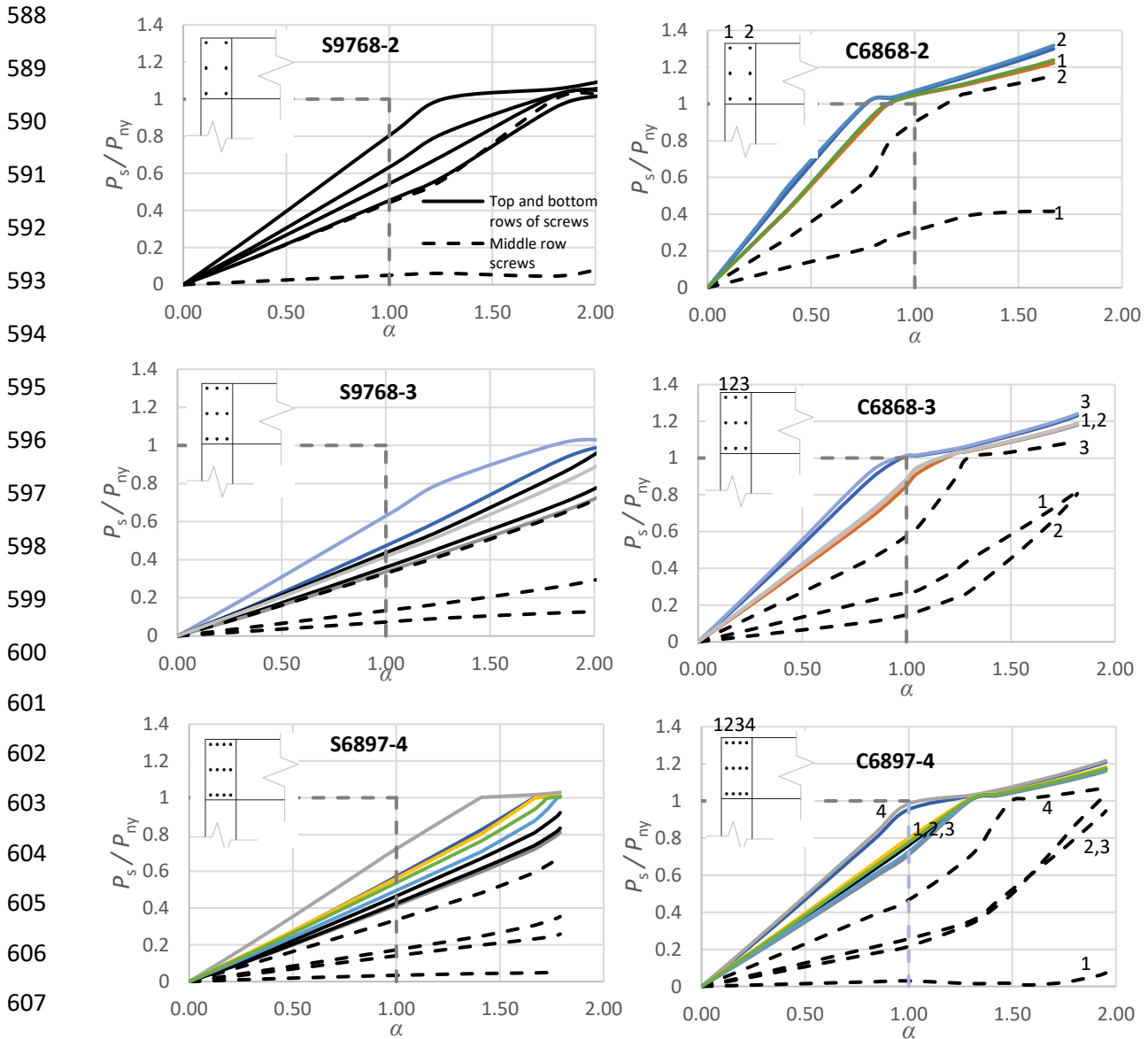
543 Fig. 16 also identifies the shear forces corresponding to each vertical lines of the screws for the CCM  
544 connections. As can be observed the last vertical line of screws from the connection end (denoted by  
545 the greatest vertical line number) attracts the greatest shear forces at each row of the screws. This is  
546 due to the superposition effect of the vertical components of the shear forces resulting from the  
547 connection shear and in-plane bending moment which are at the same and opposite directions for  
548 the last and first lines of the screws, respectively. Furthermore, the shear forces of the middle row of  
549 the screws pick up particularly after yielding of the top and bottom rows of screws which result in  
550 redistribution of the screw forces. It should be noted that the screw forces for the SCM connections  
551 follow a similar trend with more discrepancy between the top and bottom rows of screws which  
552 could be due to the more flexible nature of its supporting stud and consequential local effects  
553 compared with the CCM connections.

554



581 **Figure 15.** Variation of DCRs with  $\alpha$  for  $M$ ,  $M+V$ ,  $M+C$  and  $D$  limit states for S9768-2& 3, C6868-2& 3, S6897-4,  
 582 C6897-4, S6868-2 and S6868-3 designs.

583  
 584  
 585  
 586  
 587



609 **Figure 16.** Variation of screw shear forces with  $\alpha$  for S9768-2& 3, C6868-2& 3, S6897-4 and C6897-4 designs  
 610 (dashed lines: middle row screws, solid lines: top and bottom rows of screws).

611

612 Fig. 17 shows the von-Mises stress distribution greater than 100MPa (shown by shaded areas) for  
 613 S6897-4 and C6897-4 designs at  $\alpha = 1$ . A larger spread of shaded areas achieved for both the S6897-4  
 614 and C6897-4 joist and stud designs compared with those of the simply supported design  
 615 counterparts (shown in Fig. 11, predominantly controlled by the joist mid-span deflection), thus a  
 616 more efficient design (as reflected in Tables 4 and 5). As can be seen, the shaded areas are extended  
 617 to the studs (mainly to the compression side of the lower storey) due to the bending moment  
 618 transferred through the semi-rigid SFLS connections. This indicates the higher level of stud  $M+C$  DCR  
 619 compared with the oversized studs in simply supported connections. The simply supported



620 designs could be even more inefficient for the conventional ledger-framed designs when accounting  
 621 for the premature local failure effects (discussed in the introduction section).

622

623

624

625

626

627

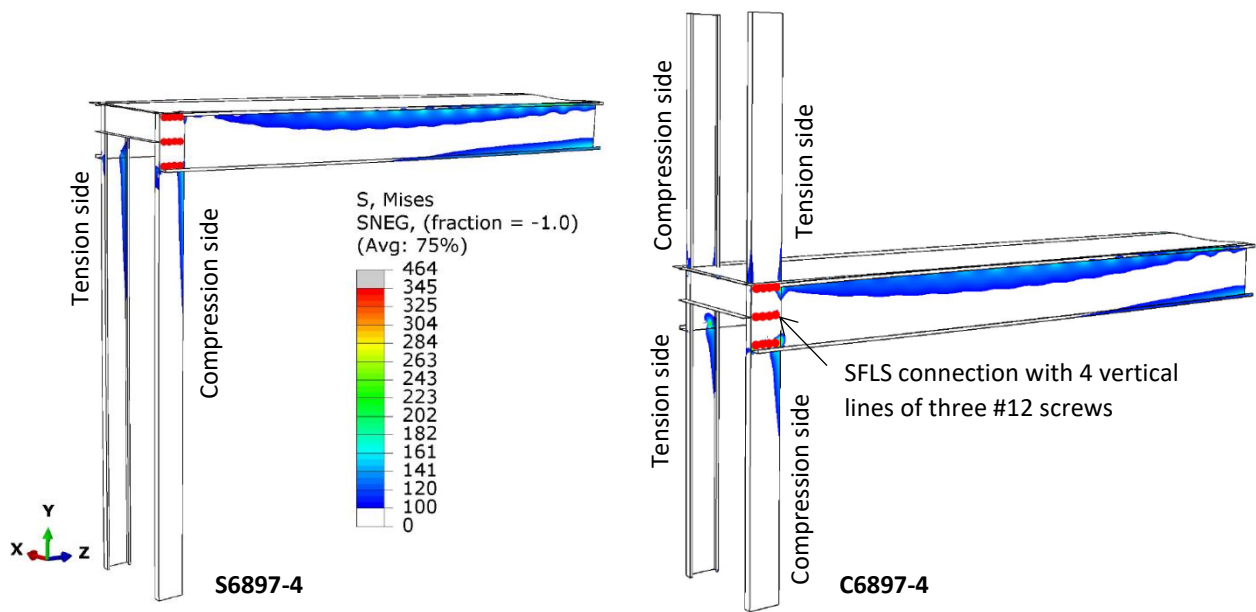
628

629

630

631

632



633 **Figure 17.** Von-Mises stress contour greater than 100 MPa for S6897-4 and C6897-4 designs at  $\alpha = 1.0$ .

634

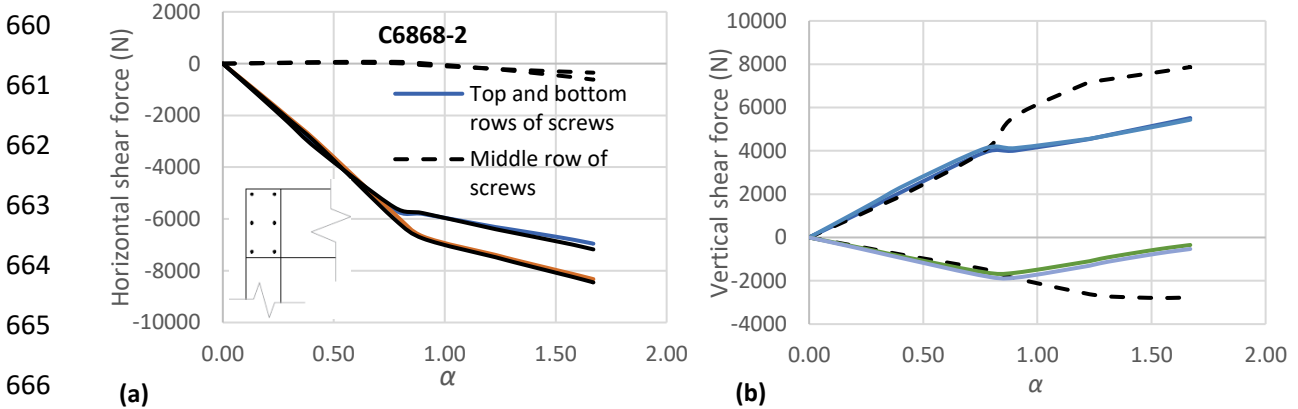
#### 635 4. Connection rotational stiffness estimation

636 As it was shown in the previous sections, the magnitude of the connection rotational stiffness has a  
 637 key role in the design of the developed semi-rigid connection for the developed SFLS system. To  
 638 calculate the SFLS connection rotational stiffness a uniform force distribution is assumed within the  
 639 joist-to-stud screw group. This can be an accurate assumption if the centre of rotation is located at  
 640 the screw group centroid and the shear force is equally distributed between the screws. Figs. 18 (a)  
 641 and 18(b) respectively show the horizontal and vertical screw force distribution of the representative  
 642 C6868-2 model. As can be seen, the top and bottom rows of screws (shown by solid lines) attract  
 643 almost the same horizontal force distribution (see Fig. 18 (a)), whilst the middle row horizontal  
 644 forces (shown by dashed lines) are close to zero. These maintain up to around  $\alpha = 0.8$  at which the  
 645 top and bottom screws reach the yielding load (which can be cross-checked with the screw forces of  
 646 C6868-2 model presented in Fig. 16). The vertical shear force distribution between the screws  
 647 (shown in Fig. 18 (b)) also shows equal shear forces distributed between the left and right vertical  
 648 lines of the screws, again up to  $\alpha = 0.8$ . Based on the horizontal and vertical screw force distribution,  
 649 it can be concluded that the uniform force distribution assumption can be utilised for the estimation  
 650 of the connection rotational stiffness before reaching the yielding load of the screws. As a design  
 651 requirement, discussed in Section 3, the yielding load of the screws is desirable to be postponed

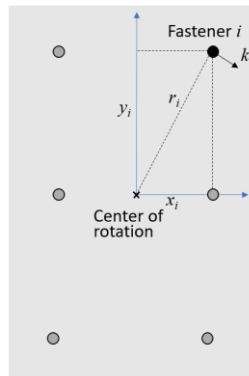
652 after  $\alpha = 1$  providing an elastic behaviour for the screws. This allows a more reliable design based on  
 653 the simplified connection rotational stiffness estimation method for the SFLS connections.

654 For the design purposes, the connection rotational stiffness,  $k_c$ , is calculated based on a uniform  
 655 screw group force distribution, using Eq. 1 and Fig. 19. This can be applicable for any arbitrary  
 656 connection arrangement having  $n$  screws located at  $x_i$  and  $y_i$  distances from the screw group centre  
 657 of rotation, while each screw has a shear stiffness of  $k_i$  in the force direction perpendicular to the  
 658 radius of  $r_i$  for that screw.

659



667 **Figure 18.** Variation of horizontal and vertical screw shear forces with  $\alpha$  for C6868-2.



668

669 **Figure 19.** Calculation of the connection rotational stiffness,  $k_c$ , for an arbitrary connection pattern.

670

$$671 \quad k_c = \sum_{i=0}^n k_i r_i^2 = \sum_{i=0}^n k_i (x_i^2 + y_i^2) \quad (1)$$

672

673 Fig. 20 shows the connection rotational stiffness of both the CCM and SCM connections having one  
 674 to four vertical lines of screws derived at  $\alpha = 1$  or just before the yielding initiates in the screws. The  
 675 estimated connection rotational stiffness,  $k_c$ , is shown by circles in Fig. 20. The connection rotational  
 676 stiffness estimations well match a linear trendline for both the SCM and CCM connections.

677  
678  
679  
680  
681  
682  
683  
684  
685  
686  
687  
688  
689  
690  
691  
692  
693  
694  
695  
696  
697  
698  
699  
700  
701  
702  
703  
704  
705  
706  
707  
708  
709

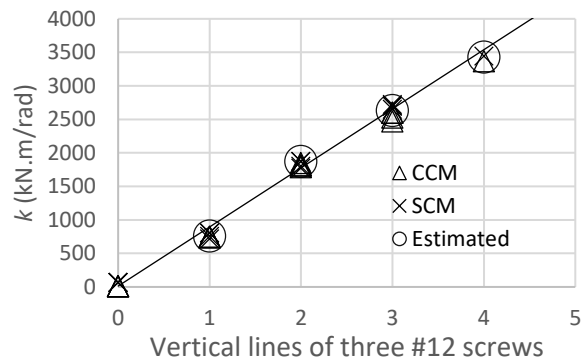


**Figure 20.** Design connection rotational stiffness,  $k_c$ , for SCM and CCM connections with one to four lines of screws.

## 5. Conclusions

Employing validated finite element (FE) analysis, a side-framed lightweight steel (SFLS) structure comprising semi-rigid floor-to-wall connections has been detailed and designed. Both the sequential and continuous construction methods (SCM and CCM) have been considered. A benchmark design having simply supported connections was chosen based on a recently tested ledger-framed floor-to-wall connections taken from the two-storey CFS-NEES project. Four design limit states were considered including the joist mid-span bending moment ( $M$ ) and deflection ( $D$ ), the joist end combined bending moment and shear force effect ( $M+V$ ) and the stud combined bending moment and compression force effect ( $M+C$ ). It was shown that the joist mid-span deflection ( $D$ ) governed the benchmark design, which is consistent with the CFS-NEES design narrative, leading to underutilised strength of the joist sections. Incorporation of even a low level of connection rotational stiffness, adopted from the ledger-framed connection tests, into the design increases the stud demand-to-capacity ratio (DCR) by up to 22%. This means an unconservative design if the connection rotational stiffness is ignored.

Variation of the joist-to-stud connection rotational stiffness,  $k$ , from zero to fully fixed condition has led to three sets of joist-stud sections corresponding to three ranges of connection rotational stiffness. SFLS connection configurations with one to four vertical lines of three #12 screws matching the identified ranges of the connection rotational stiffness were then modelled and assessed. It was shown that, in general, CCM configurations could lead to more efficient designs than those of the SCM designs with both the joist and stud limit states being dominant. The stud  $M+C$  limit state was predominant in the SCM designs within the lower range of connection rotational stiffness

710 (corresponding to one to three vertical lines of three #12 screws). This, however, can be improved  
711 by using four lines of three #12 screws leading to an efficient design (like the CCM designs). On the  
712 other hand, a higher number of screws may be required for the CCM connections compared with the  
713 SCM connections to ensure an elastic connection design.

714

715 A simplified connection rotational stiffness estimation method has been examined based on the  
716 assumption of uniform screw force distribution. It was shown that the stiffness estimations agree  
717 well with those of the FE results for both the CCM and SCM designs.

718

719 Overall, the developed SFSL system comprising semi-rigid floor-to-wall connections is expected to  
720 provide a more efficient and economical design solution compared with the conventional LSF  
721 systems. The joist and stud material strengths are more significantly utilised through the semi-rigid  
722 connections with higher DCRs as opposed to the conventional designs governed by the joist mid-  
723 span deflection and premature local failures within the connection components. The joist-stud  
724 framed designs showed a 28% lighter flooring joist sections which together with the elimination of a  
725 ledger beam per side of the walls and clip angle connections per joist could lead to a more efficient  
726 LSF system. A trade-off is, however, required for optimising the joist and stud sections in the SFSL  
727 systems varying the joist-to-stud connection rotational stiffnesses.

728

729 More experimental studies can be very beneficial to validate the provided design method. Both the  
730 design methods provided in [3] and herein, are for when the stud is not interrupted by openings  
731 between the floors. In the case of having large openings, the effect of opening on the design of joist  
732 needs further studies.

733

#### 734 **Disclaimer**

735 Any opinions, findings, and conclusions or recommendations expressed in this publication are those  
736 of the authors and do not necessarily reflect the views of the sponsors and employers.

737

#### 738 **References**

739 [1] SCI Publication P402, Light steel framing in residential construction, ISBN 13: 978-1-85942-215-1,  
740 2015.

- 741 [2] R.L. Madsen, N. Nakata, B.W. Schafer (2011). CFS-NEES Building Structural Design Narrative,  
742 Research Report, RR01, access at [www.ce.jhu.edu/cfsnees](http://www.ce.jhu.edu/cfsnees).
- 743 [3] D. Ayhan, BW. Schafer (2019). Cold-formed steel ledger-framed construction floor-to-wall  
744 connection behaviour and strength. Journal of Constructional Steel Research. 156, 215-226.
- 745 [4] AISI, North American Standard for Cold-Formed Steel Structural Framing, American Iron and Steel  
746 Institute, Washington, Dc, 2015 AISI S240.
- 747 [5] Computers and Structures INC. SAP2000 Version 20.1.0, 2018. <https://www.csiamerica.com/>.
- 748 [6] Abaqus Analysis User's Manual, (2019). version 6.21.
- 749 [7] F. Tao, A. Chatterjee, C. D. Moen (2016). Monotonic and Cyclic Response of Single Shear Cold-  
750 Formed Steel-to-Steel and Sheathing-to-Steel Connections. Virginia Tech Report No. CE/VPI-ST-16-01
- 751 [8] M. Shahini, A. Bagheri Sabbagh, P. Davidson, R. Mirghaderi (2019). Development of cold-formed  
752 steel moment-resisting connections with bolting friction-slip mechanism for seismic applications.  
753 Thin-Walled Structures, 141, 217-231.
- 754 [9] A. Bagheri Sabbagh, M. Petkovski, K. Pilakoutas K, R. Mirghaderi (2012). Development of cold-  
755 formed steel elements for earthquake resistant moment frame buildings. Thin-Walled Structures,  
756 53, 99–108.
- 757 [10] A. Fieber, L. Gardner, L. Macorini (2020). Structural steel design using second-order inelastic  
758 analysis with strain limits. Journal of Constructional Steel Research, 168, 1-19.
- 759 [11] H. Castaneda, K. Peterman (2020). Moment-rotation response of cold-formed steel joist-to-  
760 ledger connections with variable finishes in ledger-framed construction. Journal of Constructional  
761 Steel Research (In Press).